

X-ray Absorption Fine Structure Combined with X-ray Fluorescence Spectrometry. Part 15. Monitoring of Vanadium Site Transformations on Titania and in Mesoporous Titania by Selective Detection of the Vanadium $K\alpha_1$ Fluorescence

Yasuo Izumi,^{*,†} Fumitaka Kiyotaki,[†] Nobuhiro Yagi,[‡] Aurel-Mihai Vlaicu,[‡] Atsushi Nisawa,[‡] Sei Fukushima,[‡] Hideaki Yoshitake,[§] and Yasuhiro Iwasawa[⊥]

Interdisciplinary Graduate School of Science and Engineering, Tokyo Institute of Technology, Nagatsuta 4259-G1-16, Midori-ku, Yokohama 226-8502, Japan, National Institute for Research in Inorganic Materials, Kouto 1-1-1, Mikazuki-cho, Sayo, Hyogo, 679-5198, Japan, Graduate School of Environment and Information Sciences, Yokohama National University, Tokiwadai, Hodogaya, Yokohama 240-8501, Japan, and Graduate School of Science, The University of Tokyo, Bunkyo-ku, Hongo 113-0033, Japan

Received: April 20, 2005; In Final Form: May 28, 2005

X-ray absorption fine structure combined with X-ray fluorescence spectrometry was applied to various V+TiO₂ hybrid samples. Emitted V $K\alpha_1$ fluorescence from the sample was selectively counted by using a high-energy-resolution (0.4 eV) spectrometer equipped with a Ge(331) crystal. Two advantages of this method, extremely high signal/background ratio and the compatibility of measurements in the atmosphere of reaction gas (in situ study in relation to heterogeneous catalysis), were effective at the V K-edge. Structure transformation of the V sites was spectroscopically followed for the V/TiO₂ catalyst. The monooxo tetrahedral vanadate site was demonstrated to exist at 473 K. It transformed into dispersed species of 5-fold coordination in ambient air and further into polymeric VO_x species in 0.85 kPa of water at 290 K. In the presence of 3.2 kPa of 2-propanol, dissociative adsorption of 2-propanol on the dispersed V species was strongly suggested at 290–473 K. In situ structure changes of V sites on TiO₂ were reported by means of XAFS for the first time. The V^V sites for the V/TiO₂ catalysts were essentially identical with those for V supported on mesoporous (high-surface-area) TiO₂ and V–TiO₂ sample prepared by the sol–gel method. However, predominant V^{IV} sites were found for mesoporous V–TiO₂. The V^{IV} sites substituted on the Ti sites of TiO₂. When the molar ratio of V/Ti increased from 1/100 to 1/5.0, major octahedral V sites in the TiO₂ matrix looked to transform into tetrahedral ones.

Introduction

We have developed and applied a structural analysis technique, X-ray absorption fine structure (XAFS) combined with X-ray fluorescence (XRF) spectrometry, to heterogeneous catalysis and environmental chemistry.^{1–11} The fluorescence spectrometer utilized was Rowland-type¹ and the energy resolution (ΔE) was 1.1 eV at 8 keV including the contribution of beamline.⁴ Three major advantages have been demonstrated. As *advantage (1)*, this method enables a chemical/spin state-sensible structural (both geometric and electronic) study for X-ray absorbing element.^{2–4,12,13} The chemical shifts of emitted X-ray fluorescence were discriminated by high-energy-resolution XRF spectrometry. *Advantage (2)* of this method is a spectral feature of ultimately high signal/background (S/B) counts ratio.^{5–11} By suppressing the predominant background counts originating from high concentrations of element(s) in sample, weaker signals originating from lower concentrations of element were observed selectively. *Advantage (3)* is to eliminate the core-hole lifetime broadening effects by detecting the X-ray

fluorescence with a smaller energy band than the core-hole lifetime width of the X-ray absorbing K or L shell.^{2,6,10,13,14}

In this paper, vanadium K-edge XAFS combined with high-energy-resolution XRF was applied to selectively monitor low concentrations of V on/in titanium oxide. Structure transformations of the V sites were spectroscopically followed in the presence of 2-propanol or water in relation to catalysis. Advantage (2) was effective for this system^{7,8} because Ti $K\alpha_1$ (4510.8 eV), Ti $K\beta_{1,3}$ (4931.8 eV), Ti $K\beta_5$ (4962.3 eV), and/or diffracted X-ray from V+TiO₂ (VO_x–TiO₂) sample were effectively suppressed by detecting the V $K\alpha_1$ (4952.2 eV) with ΔE of 0.4 eV using a fluorescence spectrometer.^{1,8} The feasibility of advantage (3) at the V K-edge is discussed to study the preedge peak feature originating from V 1s \rightarrow 3d electronic transition in more detail. Recently by the measurements of iron $K\beta_{1,3}$ -detected XANES (X-ray absorption near-edge structure), the Fe site symmetry was discussed based on more precise separation of Fe K preedge peaks for Fe-ZSM-5 zeolites.¹⁵ In an atmosphere of reaction gas, the only way to selectively monitor minor V sites on/in high concentrations of TiO₂ matrix is selective, high-energy-resolution detection of V X-ray fluorescence associated with the V K-edge absorption.⁸

Low concentrations (less than monolayer) of VO_x supported on TiO₂ are good catalysts for the nitric oxide reduction with ammonia,¹⁶ selective oxidation of naphthalene/*o*-xylene to

* To whom correspondence should be addressed. E-mail: yizumi@chemenv.titech.ac.jp.

[†] Tokyo Institute of Technology.

[‡] National Institute for Research in Inorganic Materials.

[§] Yokohama National University.

[⊥] The University of Tokyo.

TABLE 1: The V Contents, Molar Ratio of V/Ti, and Surface VO_x Density for Various V+TiO₂ Samples

entry	sample	V content (wt %)	V/Ti molar ratio	VO _x density (nm ⁻²)
a	V/TiO ₂	3.0	1/20	7.1
b		1.0	1/63	2.4
c	mesoporous V-TiO ₂	0.6	1/100	0.059 ^a
d		10.4	1/5.0	5.4 ^a
e	V/mesoporous TiO ₂	1.0	1/63	0.18
f	sol-gel V-TiO ₂	2.0	1/31	3.9 ^a

^a Estimated values assuming all the V species dispersed on TiO₂ surface. Judging from the synthetic routes, V may be buried inside the TiO₂ matrix for these samples.

phthalic anhydride,^{17,18} and selective oxidation of butane to maleic anhydride.¹⁹ The V site structures under these catalytic reaction conditions are still controversial.²⁰ The spectroscopic (technical) difficulties in obtaining information of V sites on TiO₂ compared to on SiO₂ or Al₂O₃ were reported for XAFS,²¹ Raman (strong scattering from TiO₂),²¹ and ultraviolet (UV)-visible (strong photon absorption by TiO₂) measurements.²² Despite the technical difficulties, site structures of monomeric monoxo²¹⁻²⁵ or dioxo^{23,24,26} vanadate, polyvanadates such as decavanadate ([V₁₀O₂₈]⁶⁻),²⁷ and the change of presence ratio when these V species coexist have been reported on TiO₂ by Raman,^{21,22,27} ⁵¹V nuclear magnetic resonance (NMR),²⁵ and UV-visible spectroscopies^{21,22} and density functional theory (DFT) calculations.^{23,24} The phase similar to an epitaxial V₂O₅-(010) layer was reported to prevail over TiO₂ when the V loading was greater than 4 wt %.²⁸ The V K-edge XAFS was measured for 3.9 wt % of V on TiO₂ in the transmission mode.²⁹⁻³¹

Among various spectroscopic techniques, XAFS gives direct information on geometric and electronic structures of the V center. Thus in this paper, 0.6–10.4 wt % of V site transformations on/in TiO₂ are studied in relation to catalysis by using modern highly brilliant synchrotron X-rays and V K α ₁ XRF-combined K-edge XAFS.

Experimental Section

Sample Preparation. TiO₂ (Degussa P25; specific surface area 60 m² g⁻¹, anatase/rutile phase \approx 95/5) was impregnated with V triisopropoxide oxide (**1**) in the 2-propanol solution. These catalysts are denoted as impregnated V/TiO₂. The V contents were varied between 1.0 and 3.0 wt % on the V metal basis (1.8–5.4 wt % on the V₂O₅ basis).

Mesoporous V-TiO₂ samples were prepared from compound **1**, Ti tetraisopropoxide (**2**), and dodecylamine (**3**). An aqueous solution was maintained at 333 K for 6 days and filtered. The obtained powder was heated at 453 K for 10 days, and then washed with *p*-toluenesulfonic acid in ethanol. The V contents were varied between 0.6 and 10.4 wt %. The molar ratio of V/Ti was listed in Table 1 for each sample. The specific surface area was 1200 m² g⁻¹ for the sample of 0.6 wt % V. Based on the X-ray diffraction (XRD) analysis, the spacing of its mesopores was \approx 30 Å and wormhole-like structure prevailed rather than ordered mesoporous crystalline structure.³² Mesoporous TiO₂ prepared from compounds **2** and **3** in a similar procedure was impregnated with compound **1** in the 2-propanol solution. This sample is denoted as V/mesoporous TiO₂. Another reference sample was prepared from compounds **1** and **2** in the absence of compound **3**, in a similar procedure to that for mesoporous V-TiO₂. This sample is denoted as sol-gel V-TiO₂. All of dried powders were calcined in air at 473 K and pressed into a disk of diameter 20 mm in ambient air.

V metal foil (25 μ m-thickness, Aldrich), CrVO₄, NH₄VO₃, V₂O₅, VOSO₄·3H₂O, and V₂O₄ (Special or First Grade, Wako) were used as received. Mn_{0.9}V_{1.8}Mo_{0.2}O₆ and Mn_{0.67}V_{1.33}Mo_{0.67}O₆ crystallines were synthesized by the solid-state reaction of MnV₂O₆ with MoO₃ at 873 K.³³ The powders of these chemicals were diluted with boron nitride to 1.0 wt % V, mixed thoroughly using mortar and pestle, and pressed into a disk of diameter 20 mm.

V K α ₁ Emission and K-Edge XAFS Spectra Measurements. For the series of V+TiO₂ samples in each *fresh* state, the V K α ₁ emission spectrum was measured with the excitation energy set at 5484.1 eV using a homemade high-energy-resolution fluorescence spectrometer¹ at beamline 7C of KEK-PF. The storage ring energy was 2.5 GeV and the ring current was 390–270 mA. A Si(111) double-crystal monochromator was used. The X-ray beam was focused and fully tuned. The X-ray fluorescence from the sample was analyzed by using a spectrometer of Rowland radius set to 180 mm equipped with a Johansson-type Ge(331) crystal (50 \times 30 mm², Saint-Gobain) and a scintillation counter (SP-10, Oken). Their positions were controlled by PC on the micrometer level. After the exit of beam duct, the entire beam path was purged with helium gas except for the inside of the I₀ ion chamber (Oken; N₂:He = 3:7).^{1,4}

The fluorescence spectrometer was tuned to the peak top for each sample and the V K-edge XAFS spectrum was measured at 290 K. The scan step of the monochromator was \sim 6.9, \sim 0.25, and \sim 2.75 eV in the energy range 5130–5440, 5440–5545, and 5545–6015 eV, respectively. The dwell time of each data point was 60–200 s. The energy positions of the monochromator and the fluorescence spectrometer were reproduced within \pm 0.1 and \pm 0.2 eV, respectively. The V K α ₁ and V K rising-edge energies of the V metal were calibrated to 4952.20 and 5463.9 eV, respectively.³⁴ The XAFS spectra for standard inorganic V compounds were measured in transmission mode at 290 K using an I₁ ion chamber purged with N₂ instead of the high-energy-resolution fluorescence spectrometer.

In situ V K α ₁-detecting XAFS measurements for V/TiO₂ catalyst were performed at beamline 15XU of SPring-8.³⁵ The storage ring energy was 8.0 eV and the ring current was 89–53 mA. A Si(111) double-crystal monochromator was used. The planer undulator gap and the $\Delta\theta$ of the second crystal of the monochromator (rocking curve) were optimized to maximize the beam flux at each data point of the XAFS spectrum scan. The scan steps and the setup and measurement conditions of the fluorescence spectrometer were essentially the same as those for the measurements at KEK-PF. The fluorescence spectrometer was tuned to the top of the V K α ₁ peak and then the XAFS spectrum was measured. The dwell time of each data point was 10–60 s. The pressed disk of V/TiO₂ (1.0 wt % V) was introduced into a reaction cell made of stainless steel, equipped with two Be windows for incident and emitted X-rays, ceramic heater, water cooling path, gas supply, and a connection to a vacuum pump. The two Be windows of 100 μ m thickness and 10 mm diameter were located to make an angle of $\pi/2$ projected from the sample at the center of the reaction cell. The sample temperature can be controlled between 290 and 673 K. The reaction cell was accommodated in our high-energy-resolution fluorescence spectrometer for spectral measurements. After the reaction cell was evacuated, 3.2 kPa of 2-propanol or 0.85 kPa of water was introduced.

XAFS Data Analysis. The XAFS data analysis was performed with the package XDAP (XAFS Services International) based on the works of M. Vaarkamp, H. Linders, and D.

TABLE 2: Local Structure Information of the V Sites for Standard Inorganic V Compounds

	formal valence	bond type	no. of bonds	bond distance (Å)	ref
CrVO ₄	5	V–O	4	1.72 × 2, 1.80 × 2	37
NH ₄ VO ₃	5	V–O	4	1.66 × 2, 1.81 × 2	37
V ₂ O ₅	5	V–O	5	1.585, 1.780, 1.878 × Z2, 2.021	37
Mn _{1-x} V _{2-2x} Mo _{2x} O ₆ (<i>x</i> = 0.53)	5	V–O	5	1.661, 1.693, 1.913, 1.930, 2.151	33
VOSO ₄ ·3H ₂ O	4	V–O	1	1.56	37
		V–OSO ₃	2	2.02 × 2	
		V–OH ₂	2	2.05, 2.08	
		V–O	6	1.76, 1.86, 1.87, 2.01, 2.03, 2.05	
V ₂ O ₄	4	V–O	6	1.76, 1.86, 1.87, 2.01, 2.03, 2.05	37
[V ₁₀ O ₂₈] ⁶⁻	5	(eight V atoms)	6	1.61, (1.83–2.05) × 4, 2.23–2.34	38
		(two V atoms)	6	1.61, (1.83–2.05) × 4, 2.23–2.34	
		V–O	6	1.70 × 2, 1.93 × 2, 2.12 × 2	

Koningsberger. The preedge background was approximated by the modified Victoreen function

$$\frac{C_2}{E^2} + \frac{C_1}{E} + C_0$$

The preedge peak energy position, width, and intensity were evaluated by the fit of the pseudo-Voigt function³⁶ using KaleidaGraph version 3.6.4 (Synergy Software). The intensity ratio of the Lorentzian and Gaussian components was fixed to 1:1. The background of EXAFS (extended X-ray absorption fine structure) oscillations was approximated by a smoothing spline function calculated by the equation for the number of data points *N*

$$\sum_{i=1}^N \frac{(\mu x_i - BG_i)^2}{\exp(-0.075k_i^2)} \leq \text{smoothing parameter}$$

Multiple shell curve-fit analyses were performed for the Fourier-filtered EXAFS data using empirical parameters for V–O extracted from EXAFS for CrVO₄. The bond distance and coordination number were based on the crystal structure for CrVO₄ (Table 2).³⁷ The σ^2 values are listed relative to that for this model. The many-body reduction factor (S_0^2) was assumed to be equal for sample and reference. The goodness of fit was given as requested by the Committee on Standards and Criteria in X-ray Absorption Spectroscopy.

Results

V K α_1 Emission Spectra. The V K α_1 emission peaks for all V+TiO₂ samples appeared at 4951.5–4952.0 eV.⁸ The chemical shifts with respect to V metal were reported at –0.1, –0.3 to –0.4, and –0.5 to –0.6 eV for V^{III}, V^{IV}, and V^V compounds, respectively.³⁹ Hence, the V valence states in V+TiO₂ samples studied in this paper were IV and/or V.

XANES of V/TiO₂. Normalized V K-edge XANES spectra are shown in Figure 1. The intensity and energy positions for the preedge peak and rising edge were summarized in Table 3. For impregnated V/TiO₂ (Figure 1a,b), the rising edge appeared at 5480.8–5481.1 eV. Among data for reference inorganic V compounds (spectra g–l), the rising edge position for Mn_{0.9}V_{1.8}Mo_{0.2}O₆ (g) or NH₄VO₃ (i) was most close to the values for V/TiO₂. The spectrum for Mn_{0.67}V_{1.33}Mo_{0.67}O₆ (not shown) was essentially the same as that for Mn_{0.9}V_{1.8}Mo_{0.2}O₆ (g). Two broad peak features were observed in the postedge region (5489 and 5502 eV) at nearly equal intensity in spectra a and b. The two peak energy positions were similar to 5489 and 5503 eV for V/TiO₂ (3.9 wt % V; f)³¹ and 5490 and 5504 eV for Mn_{0.9}V_{1.8}Mo_{0.2}O₆ (g). Mn_{1-x}V_{2-2x}Mo_{2x}O₆ (0 < *x* < 1) consists

of a Brannerite-type crystal structure.⁴⁰ The V site was coordinated by two nearer O atoms (1.661–1.693 Å) and three farther O atoms (1.913–2.151 Å) when the *x* value was 0.53 (Table 2).³³ A shoulder peak appeared at 5486 eV in Figure 1b,g. The postedge patterns for CrV^{VO}O₄ (h), NH₄V^{VO}O₃ (i), and V^VO₅ (j) were qualitatively different from those of spectra a and b.

A 1s → 3d preedge peak appeared at 5468.3–5468.6 eV for V/TiO₂ (Figure 1 and Table 3) at similar energy positions to those for Mn_{0.9}V_{1.8}Mo_{0.2}O₆, CrVO₄, and NH₄VO₃ (5468.2–5468.6 eV). However, the peak intensity for spectra a and b was only 62–70% of that for CrVO₄ (h). This difference suggests that the V site symmetry for V/TiO₂ (1.0–3.0 wt % V) was higher than tetrahedral for the V sites of CrVO₄ and NH₄VO₃. The preedge peak intensity was comparable between V/TiO₂ (Table 3, entries a and b) and Mn_{0.9}V_{1.8}Mo_{0.2}O₆ (Table 3, entry g) within the difference of 20%.

XANES of Mesoporous V–TiO₂, V/Mesoporous TiO₂, and Sol–Gel V–TiO₂. For mesoporous V–TiO₂ (0.6 wt % V), the rising edge position shifted by 1.0–1.3 eV toward the lower energy side compared to data for V/TiO₂ (Table 3, entries a–c). This shift suggested the dominance of V^{IV} and V^V sites for mesoporous V–TiO₂ and impregnated V/TiO₂, respectively, based on rising edge energy positions for standard V^{IV} (Table 3, entries k and l) and V^V (Table 3, entries g–j) compounds

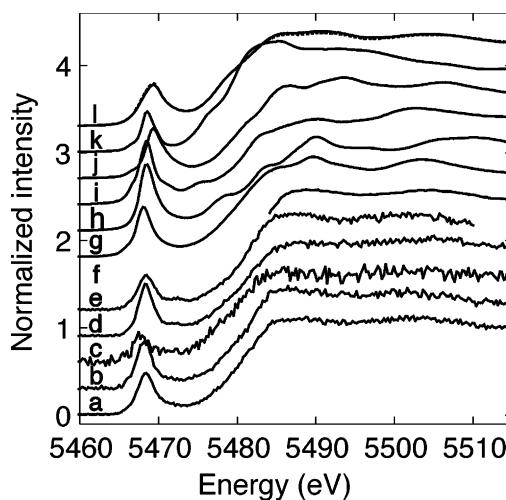


Figure 1. V K-edge XANES spectra for several V+TiO₂ samples combined with high-energy-resolution XRF (a–e). Impregnated V/TiO₂ of 3.0 (a) and 1.0 wt % V (b), mesoporous V–TiO₂ (0.6 wt % V; c), V/mesoporous TiO₂ (1.0 wt % V; d), and sol–gel V–TiO₂ (2.0 wt %; e). Reference V K-edge XANES spectra (f–l) measured in transmission mode for V/TiO₂ (3.9 wt % V; f),³⁰ Mn_{0.9}V_{1.8}Mo_{0.2}O₆ (g), CrVO₄ (h), NH₄VO₃ (i), V₂O₅ (j), VOSO₄·3H₂O (k), and V₂O₄ (l). Spectrum l' (dotted line) was measured in fluorescence detection mode with a Lytle detector.

TABLE 3: The Intensity and Energy Position of Preedge Peaks and the Energy Position of Rising Edge for Various V+TiO₂ Samples and Standard Inorganic V Compounds^a

entry	sample	V content (wt % V)	preedge peak			rising edge
			intensity	fwhm (eV)	energy (eV)	energy (eV)
a	V/TiO ₂	3.0	0.47	2.5	5468.6	5480.8
b		1.0	0.53	2.5	5468.3	5481.1
c	mesoporous V-TiO ₂	0.6	0.32	2.3	5467.9	5479.8
d		10.4	0.80	2.4	5468.2	5479.7
e	V/mesoporous TiO ₂	1.0	0.59	2.4	5468.5	5481.1
f	sol-gel V-TiO ₂	2.0	0.39	2.5	5468.5	5481.3
g	Mn _{0.9} V _{1.8} Mo _{0.2} O ₆		0.57	2.4	5468.2	5480.5
h	CrVO ₄		0.76	2.3	5468.6	5482.2
i	NH ₄ VO ₃		0.73	2.3	5468.6	5481.3
j	V ₂ O ₅		0.57	2.5	5469.5	5480.0
k	VOSO ₄ ·3H ₂ O		0.46	2.2	5468.8	5479.8
l	V ₂ O ₄		0.47	3.4	5469.4	5477.5
l'	V ₂ O ₄ ^b		(0.49)	(3.4)	(5469.4)	(5477.5)
m	mesoporous TiO ₂		0.25	3.0	4968.1	4978.4

^a Entries a–f were for XAFS spectra combined with high-energy-resolution XRF. Entries g–m were measured in transmission mode. ^b Entry l' was measured in fluorescence detection mode with a Lytle detector.

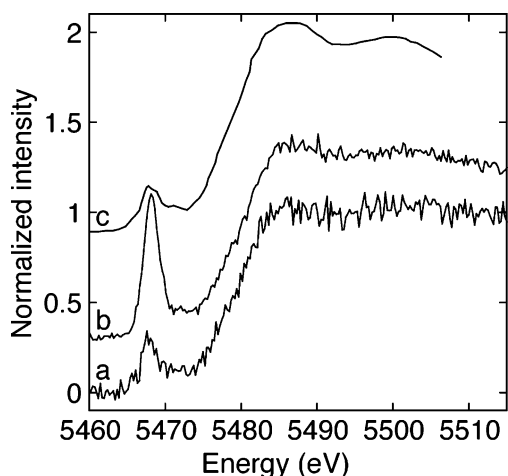


Figure 2. V K-edge XANES spectra for mesoporous V-TiO₂ samples combined with high-energy-resolution XRF. V contents: 0.6 (a) and 10.4 wt % (b). Reference Ti K-edge XANES measured in transmission mode for mesoporous TiO₂ (c). The energy of spectrum c was shifted by +499.8 eV for comparison to V K-edge spectra.

and data in the literature.³⁷ Two broad peak features were observed at 5487 and 5505 eV in the postedge region, shifted by ± 2 eV from the values for V/TiO₂. Although the rising edge position for V^{IV}O₄·3H₂O was identical with that for mesoporous V-TiO₂, the postedge pattern was totally different between the two (Figure 1c,k). The postedge pattern for V^{IV}O₄ (l) was relatively similar to that for spectrum c. The Ti K-edge spectrum for mesoporous TiO₂ was compared to V K-edge spectra by shifting the former energy scale by +499.8 eV to adjust the preedge peak energy. The phase parameters are similar between Ti and V. The rising edge energy position and postedge pattern were very alike those of V K-edge for mesoporous V-TiO₂ (Figure 2a,c).

The preedge peak intensity and energy position for VOSO₄·3H₂O and V₂O₄ were not comparable to those for mesoporous V-TiO₂ (Table 3, entries c, k, and l). The Ti K preedge peak intensity for mesoporous TiO₂ was comparable to that for the V K preedge peak for mesoporous V-TiO₂. These preedge peak intensities (0.32 and 0.25) were 53–68% of that for V₂O₄. The V^{IV} sites of V₂O₄ are coordinated by three nearer O atoms (1.76–1.87 Å) and three further O atoms (2.01–2.05 Å) (Table 2).³⁷ Thus, the V site symmetry was suggested to be even higher for mesoporous V-TiO₂ than that for V₂O₄. The full-width at half-maximum (fwhm) value of the preedge peak for

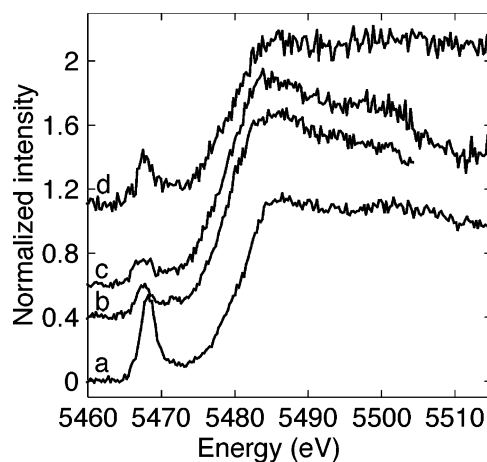


Figure 3. In situ V K-edge XANES spectra for V/TiO₂ (1.0 wt % V) combined with high-energy-resolution XRF: as prepared (a), in 3.2 kPa of 2-propanol at 290 (b) and 473 K (c), and mesoporous V-TiO₂ (0.6 wt % V) for comparison (d).

mesoporous V-TiO₂ (2.3 eV) was smaller than those for V/TiO₂ (2.5 eV). This implies that the V sites in mesoporous V-TiO₂ are more statistically uniform compared to those in V/TiO₂ because the spectral measurement conditions for these samples were essentially the same. In summary, the local structure of predominant V^{IV} species in mesoporous V-TiO₂ was more uniform and similar to that of Ti sites in mesoporous TiO₂.

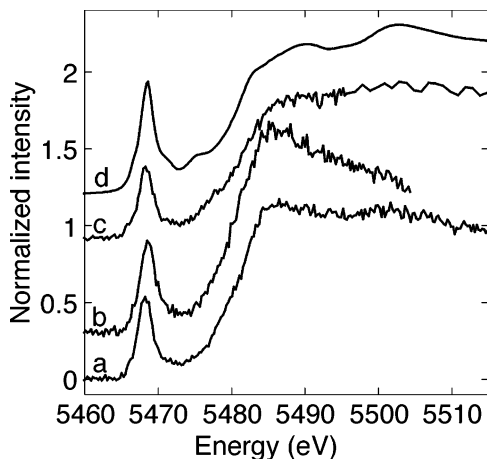
The XANES spectrum for mesoporous V-TiO₂ that contains more V content (10.4 wt % V) by 20 times is depicted in Figure 2b. The spectrum was very similar to those for mesoporous V-TiO₂ (0.6 wt % V) and mesoporous TiO₂ (spectra a and c) except for a more intense preedge peak by 2.5–3.2 times (Table 3, entry d). For V/mesoporous TiO₂ and sol-gel V-TiO₂, the preedge, rising edge, and two postedge-region peaks appeared at 5468.5, 5481.1–5481.3, 5487–5488, and 5501–5504 eV, very close to those for impregnated V/TiO₂ (5468.3–5468.6, 5480.8–5481.1, 5489, and 5502 eV). Preedge peak intensities for V/mesoporous TiO₂ and sol-gel V-TiO₂ were 111–126% and 74–83%, respectively, compared to values for V/TiO₂ (Table 3). Thus, the V sites of these two reference samples were essentially the same as those of V/TiO₂.

In Situ XANES of V/TiO₂. In situ V K-edge XANES spectra in 3.2 kPa of 2-propanol were measured by selectively detecting the V K α_1 signals (Figure 3 and Table 4). The spectra measured at 290 and 473 K in the reaction cell were similar to

TABLE 4: Changes of Intensity and Energy Position of Preedge Peaks and the Energy Position of Rising Edge for V/TiO₂ (1.0 wt % V, a–c) in the Presence of 2-Propanol (3.2 kPa)^a and Reference Spectrum Data (d)

entry	conditions	preedge peak		rising edge	
		intensity	fwhm (eV)	energy (eV)	energy (eV)
a	once exposed in air, 290 K	0.53	2.5	5468.3	5481.1
b	in 2-propanol, 290 K	0.20	2.5	5467.7	5479.9
c	in 2-propanol, 473 K	0.18	2.6	5467.7	5479.5
d	mesoporous V–TiO ₂ (0.6 wt % V)	0.32	2.3	5467.9	5479.8

^a Entries a–d were for XAFS spectra combined with high-energy-resolution XRF.

**Figure 4.** In situ V K-edge XANES spectra for impregnated V/TiO₂ (1.0 wt % V) combined with high-energy-resolution XRF: as prepared (a) and in 0.85 kPa of water at 290 (b) and 473 K (c). Data for NH₄VO₃ were measured in transmission mode for comparison (d).

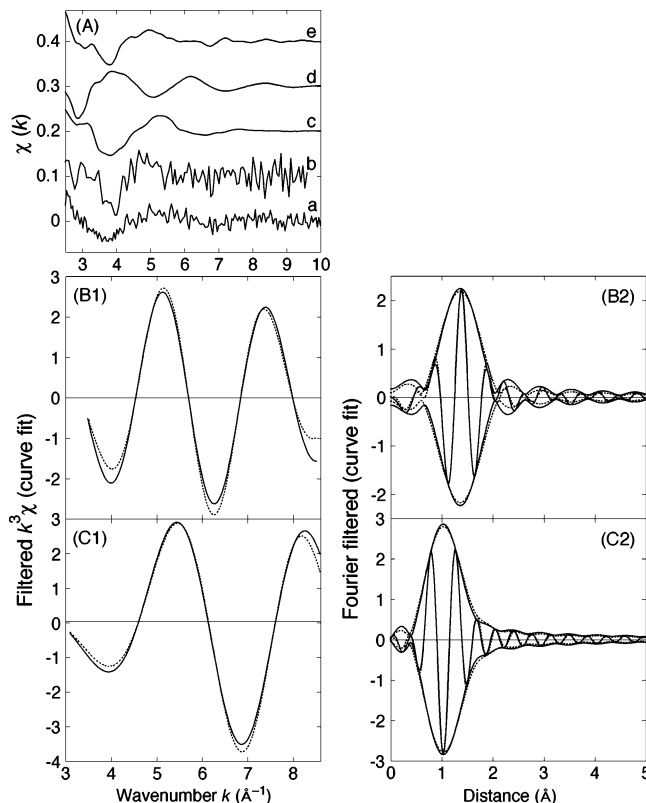
each other (Figure 3b,c). The preedge peaks became weaker 34–38% and shifted toward the lower energy side by 0.6 eV with respect to the peak for fresh sample (Table 4). The rising edge energy position also shifted toward the lower energy side by 1.2–1.6 eV. The postedge broad peaks at 5489 and 5502 eV for fresh sample shifted to 5486 and 5501 eV in 2-propanol. The former peak became more intense than the latter (Figure 3b,c). The values of intensity, width, and energy position of preedge peak, rising edge energy position, and the two postedge broader peak positions for spectra of V/TiO₂ in 2-propanol (Table 4, entries b and c) were similar to corresponding values for mesoporous V–TiO₂ of 0.60 wt % V (Table 4, entry d, and Figure 3d).

In situ V K-edge XANES spectra for V/TiO₂ measured in 0.85 kPa of water are depicted in Figure 4. Representative data values are summarized in Table 5. At 290 K, the preedge peak negligibly changed compared to the fresh one, but the rising edge shifted toward the lower energy side by 0.9 eV and the intense postedge peak appeared at 5486 eV (Figure 4b). This V species is not identical with that postulated to exist in 2-propanol (Figure 3b,c) because the preedge peak intensities were different by 3.0–3.3 times (Table 4, entries b and c, and Table 5, entry b). At 473 K, the preedge peak was still negligibly changed. On the contrary, the postedge region qualitatively changed. The broad peak at 5506 eV became more intense compared to that at 5489 eV (Figure 4c). The most similar spectrum profile to this was found for NH₄VO₃ (d). The transformation of V species corresponding to Figure 4a into 4c was reversible. A very similar spectrum

TABLE 5: Changes of Intensity and Energy Position of Preedge Peaks and the Energy Position of Rising Edge for V/TiO₂ (1.0 wt % V, a–c) in the Presence of Water (0.85 kPa)^a and Reference Spectrum Data (d)

entry	conditions	preedge peak		rising edge	
		intensity	fwhm (eV)	energy (eV)	energy (eV)
a	once exposed in air, 290 K	0.53	2.5	5468.3	5481.1
b	in water, 290 K	0.59	2.5	5468.7	5480.2
c	in water, 473 K	0.47	2.5	5468.4	5482.1
d	NH ₄ VO ₃	0.73	2.3	5468.6	5481.3

^a Entries a–c were for XAFS spectra combined with high-energy-resolution XRF. Entry d was measured in transmission mode.

**Figure 5.** V K-edge EXAFS. (A) $\chi(k)$ functions for fresh mesoporous V–TiO₂ (10.4 wt % V) (a), V/TiO₂ (1.0 wt % V) in 0.85 kPa of water at 473 K (b), NH₄VO₃ (c), VOSO₄·3H₂O (d), and Mn_{0.9}V_{1.8}Mo_{0.2}O₆ (e). Best fits for filtered k^3 -weighted χ -functions of V/TiO₂ (B) and mesoporous V–TiO₂ (C) both in k -space (1) and R -space (2); the magnitude and imaginary parts: (—) experiment and (---) theory.

to spectrum a was obtained when the sample for spectrum c was cooled to 290 K, evacuated, and exposed to ambient air.

EXAFS. V K α_1 -detecting EXAFS spectra were measured for V/TiO₂ (1.0 wt % V) in 0.85 kPa of water at 473 K and mesoporous V–TiO₂ (10.4 wt % V). The background-subtracted EXAFS χ -functions are depicted in Figure 5A (b and a, respectively) along with those for reference compounds, NH₄VO₃ (c), VOSO₄·3H₂O (d), and Mn_{0.9}V_{1.8}Mo_{0.2}O₆ (e). The χ -functions a–c were relatively similar in this k -range. The best-fit results for filtered k^3 -weighted χ -functions in both k -space and R -space are depicted in Figure 5, parts B and C, and the data are listed in Table 6. Only one-wave fits were performed due to the limited available k -range of data. For both samples, the coordination number of V–O bonds was found to 3–4. The

TABLE 6: Best-Fit Results of V K-edge EXAFS Combined with V K α_1 -Detecting Fluorescence Spectrometry for V/TiO₂ (1.0 wt % V) and Mesoporous V-TiO₂ (10.4 wt % V)^a

sample	V-O			goodness of fit
	<i>N</i>	<i>R</i> (Å)	$\Delta(\sigma)^2$ (Å ²)	
V/TiO ₂ in water, 473 K	3.4(±0.7)	1.863(±0.018)	-0.0016(±0.0019)	674
Mesoporous V-TiO ₂ , once exposed in air	4.1(±0.6)	1.667(±0.017)	0(±0.0014)	360

^a Values in parentheses are estimated fit errors.

average V-O bond distance was shorter for mesoporous V-TiO₂ (1.67 Å) than that for V/TiO₂ in water at 473 K (1.86 Å).

Discussion

Advantages of V K α_1 -Detecting XAFS. V K α_1 -detecting V K-edge XAFS spectra were obtained for various fresh V+TiO₂ samples (Figure 1). The application of this technique was extended to V/TiO₂ catalyst in two kinds of reaction gas at elevated temperature (Figures 3–5). In addition to advantage (2) (see the Introduction section), selective V K α_1 detection is advantageous compared to selective Auger or secondary photoelectron detection derived from V sites by an electron energy analyzer because X-ray fluorescence-detecting XAFS is compatible with the presence of reaction gases.

In V K-edge XANES spectra, the preedge peak width is related to the core-hole lifetime width of *K* + *M*_{4or5} (≈ 1.01 eV),⁴¹ the ΔE of the beamline, the energy splitting of the unoccupied V 3d multiplet to which the 1s electron can transit, and the peak energy variation due to the presence of some kinds of V sites in a sample. The last factor is negligible in the case of VOSO₄·3H₂O crystalline. A general trend exists that the width of the preedge peak decreased as the coordination number to V decreased (accordingly smaller *10Dq* values) for standard inorganic V compounds (Tables 2 and 3). Thus, the latter two factors should be minimal for the spectra of VOSO₄·3H₂O, CrVO₄, and NH₄VO₃. Their preedge peak widths were smallest (2.2–2.3 eV, Table 3). Therefore, the total energy width due to ΔE of the beamline and the latter two additional factors was estimated to 2.0 eV.

The V K α_1 emission peak width is related to the core-hole lifetime width of *K* + *L*₃ (1.26 eV),⁴¹ the ΔE of the beamline and of fluorescence spectrometer, and the peak energy variation due to the presence of some kinds of V sites in sample. The smallest fwhm values for the V K α_1 peak were 2.4 eV for V metal and impregnated V/TiO₂.⁸ If we assume the V 3d multiplet splitting effect (for vacant levels to which the 1s electron transits) on the V preedge peak width was negligible, the ΔE of our fluorescence spectrometer is estimated to 0.4 eV at 5 keV.

To apply advantage (3) (the Introduction section) at the V K-edge, the convolution of ΔE of the beamline and fluorescence spectrometer should be less than the core-hole lifetime width of vanadium K (1.01 eV). To satisfy this condition, the ΔE of the beamline should be less than 0.9 eV. Thus, advantage (3) was not effective in this paper. The fact is evident in Table 3 that the preedge peak widths for V K α_1 -detecting XAFS using a fluorescence spectrometer (2.3–2.5 eV, a–e) were comparable to those for spectra measured in transmission mode (2.2–3.4 eV, g–l).

V Site Structure Transformations. Olthof et al.²¹ reported XANES for supported V samples over SiO₂, Al₂O₃, ZrO₂, and HfO₂ under hydrated and dehydrated conditions. The V K-edge data were measured in conventional fluorescence detection mode.⁴² Reported XANES profile changes before and after dehydration in dry air at 723 K for V/SiO₂ (8.4 wt % V) and

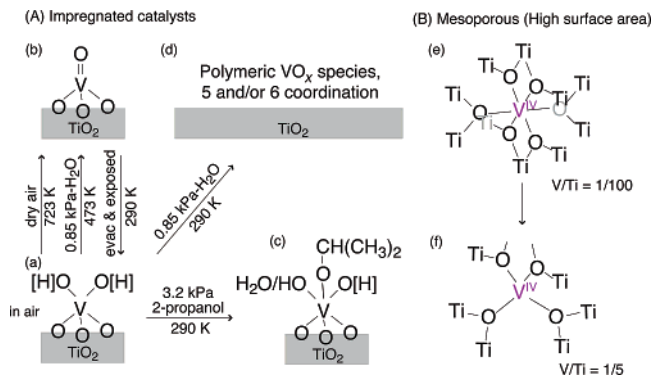


Figure 6. Proposed V site transformations for V/TiO₂ in reactant/product gas (A) and for mesoporous V-TiO₂ by changing the molar ratio of V/Ti (B). [H] for models a and c indicates the presence/absence of hydrogen cannot be determined.

V/Al₂O₃ (5.6 wt % V) in ref 21 were similar to the change observed in this paper before and after the water (0.85 kPa) treatment at 473 K for V/TiO₂ (1.0 wt % V) (Figure 4a,c). Postedge profile changes were remarkable in both cases.

Structural change by dehydration of V/TiO₂ (0.6–2.2 wt % V) was studied using ⁵¹V NMR⁴³ and Raman.²⁷ Upon dehydration, transformation from 6-fold coordination polymeric vanadate (e.g. metavanadate) into dispersed tetrahedral monooxo vanadate was suggested. The V site transformation from higher symmetry to tetrahedral was supported by DFT calculations^{23,24,44} and ab initio calculations of V K-edge XANES spectra.⁷ Spectrum profiles of Figure 4a and 4c were more similar to data for surface V site models of 5-fold and 4-fold coordination, respectively, calculated by ab initio calculations of XANES.⁷ V K α_1 -detecting EXAFS analysis demonstrated V-O bonds at 1.86 Å (average) with the coordination number of 3–4 rather than 5 (Table 6) for V/TiO₂ in water at 473 K. Thus, the V sites of V/TiO₂ in water at 473 K (Figures 4c, 5A-b, and 5B) are determined for monooxo (distorted) tetrahedral species (Figure 6b).

Monooxo tetrahedral V species were reported over SiO₂, Al₂O₃, and TiO₂ based on a V=O stretching Raman peak at ≈ 1030 cm⁻¹ in comparison with data for standard compounds (O=V)X₃ (X = halogens and alkoxides).^{21,45} Jehng et al. reported the effects of water on the V site structure for V/TiO₂ (0.56 wt % V) as a function of temperature using Raman spectroscopy.⁴⁶ In moisture, the peak at 1024 cm⁻¹ was observed between 623 and 723 K but it diminished between 393 and 443 K. This trend does not contradict with our results in Figure 4. Namely, (distorted) monooxo tetrahedral V species in spectrum c measured at 473 K in water transformed into the V species of higher symmetry until 290 K (spectrum a). Proposed V site transformation was illustrated in Figure 6 (b → a → d).

The XANES spectrum for fresh V/TiO₂ (Figure 1b) was measured inside the acrylic chamber of the fluorescence spectrometer purged with He gas; however, the sample was once exposed to ambient air before the measurement. The XANES was most similar to that for Mn_{1-x}V_{2-2x}Mo_{2x}O₆ (Figure 1g and

Table 3, entry g) in which the V sites are 5-fold coordinated (Table 2).³³ The V–OH bond length is reported between 1.75 and 1.85 Å^{23,44,47} versus V–O bond lengths for standard V compounds listed in Table 2. Therefore, dispersed vanadate species of 5-fold coordination are proposed for *fresh, exposed* V/TiO₂ transformed from monooxo V species (Figure 6, b → a). The extent of hydration for the V species of Figure 1b should be intermediate. When the V/TiO₂ sample was in 0.85 kPa of water at 290 K (Figure 4b), the dispersed vanadate species (Figure 6, a and/or b) was thoroughly hydrated to transform into surface polymerized species (d).^{21,22,27,46,48} For V/TiO₂ in ambient condition, a higher ratio of polymeric vanadate versus dispersed tetrahedral monooxo vanadate was reported compared to the cases of V/SiO₂ and V/Al₂O₃ in ambient condition.²¹ Hence, species a and d illustrated in Figure 6 may coexist for ambient V/TiO₂ (1.0–3.0 wt % V) in this study. Even if the V sites were the mixture, the V sites of 5-fold coordination should be dominant because the XANES spectra (Figure 1a,b) were most similar to that for Mn_{0.9}V_{1.8}Mo_{0.2}O₆ (Figure 1g).

In situ V K-edge XANES for V/TiO₂ in 2-propanol (3.2 kPa) both at 290 and 473 K suggested higher coordination (higher symmetry) V sites (Figure 3b,c). Hence, dissociative adsorption of the 2-propanol molecule on dispersed vanadate was suggested to form octahedral vanadate species (Figure 6c). Went et al. observed the reaction of V/SiO₂, V/Al₂O₃, and V/TiO₂ with ethanol by Raman. They discussed that with the addition of ethanol the cleavage of the V–O–M bond proceeded when M = Si but simple adsorption of ethanol was proposed when M = Al and Ti.⁴⁹ The transformation proposed in Figure 6a,c is consistent with their discussion.

Varieties of V Sites On/Inside TiO₂. In the series of V+TiO₂ samples, only the V sites of mesoporous V–TiO₂ were found to be at the V^{IV} state and the local site structure was similar to that for Ti sites of mesoporous TiO₂ (Figure 2a,c). The V^{IV} sites should be substituted on the Ti sites (Figure 6e). The reason is unclear why only the preedge peak intensity grew by 2.5 times (Table 3, entry d) when the V content increased from 0.6 to 10.4 wt % (molar ratio of V/Ti increased from 1/100 to 1/5.0) in spite that other spectral profiles were essentially retained (Figure 2a,b). The preedge peak intensity for mesoporous V–TiO₂ (10.4 wt % V) was close (105–110%) to those for the tetrahedral V sites of CrVO₄ and NH₄VO₃ (Table 3, entries d, h, and i). One of the plausible explanations for this preedge peak intensity change is that major octahedral V sites in the case of 0.6 wt % V in the TiO₂ matrix switched to tetrahedral ones for mesoporous V–TiO₂ of 10.4 wt % V (Figure 6f). This possibility was supported by V Kα₁-detecting EXAFS analysis for the 10.4 wt % V sample (Figure 5A-a and C). The coordination number was evaluated to four for the V–O bonds (Table 6). The bonding distance was relatively short (1.67 Å).

V site incorporation within the TiO₂ (anatase) matrix was reported for sol–gel V–TiO₂ based on XRD, X-ray photoelectron spectroscopy, electron spin resonance, and ⁵¹V NMR measurements.⁵⁰ The molar ratio V/Ti was varied between 1/50 and 1/17 in ref 50. The molar ratio of V/Ti for sol–gel V–TiO₂ synthesized in the absence of template molecule in this paper was comparable (1/31, Table 1). However, dispersed V species over TiO₂ surface were proposed based on V Kα₁-detecting XAFS, similar to the V species for impregnated V/TiO₂ and V/mesoporous TiO₂ (Figures 1 and 6A). The difference in the calcination temperatures (723–1173 K in ref 50 and 473 K in this work) may be the reason of different distribution of V on/inside TiO₂.

Conclusions

V Kα₁-detecting K-edge XAFS spectra were measured for V/TiO₂ (1.0–3.0 wt % V), mesoporous V–TiO₂ (0.6–10.4 wt % V), V/mesoporous TiO₂ (1.0 wt % V), and sol–gel V–TiO₂ (2.0 wt % V). Owing to the selective detection of V Kα₁ fluorescence associated with the V K-edge absorption with the energy resolution of 0.4 eV, spectra of extremely high *S/B* ratio were obtained. The data were free from the effects of high concentrations of Ti and measurements in the presence of 3.2 kPa of 2-propanol or 0.85 kPa of water were also enabled. These gases are reactant and product in the catalysis (selective reduction of NO and selective oxidation to phthalic hydride and maleic anhydride).

Dispersed 5-fold coordination vanadate and/or surface polymeric VO_x species of 5-fold coordination were found for V/TiO₂ once exposed to ambient air. In the presence of 0.85 kPa of water, the species should be transformed thoroughly into polymerized species at 290 K whereas reverse transformation to monooxo (distorted) tetrahedral vanadate was observed at 473 K. This temperature dependence of V site structure in moisture was consistent with literature based on Raman spectroscopy.⁴⁶ Dissociative adsorption of 2-propanol to the dispersed vanadate was suggested to constitute (nearly) octahedral V sites at 290–473 K. This was consistent with literature where different reactivities of the V–O–M (M = Si, Al, and Ti) bond with ethanol were discussed based on Raman spectroscopy.⁴⁹ As far as our V+TiO₂ samples were preheated to 473 K in air, the V^V site structures seem to be common for V/TiO₂, V/mesoporous TiO₂, and sol–gel V–TiO₂. An exception was the V^{IV} species dominant for mesoporous V–TiO₂. The V sites substituted on the Ti sites of high-surface-area TiO₂.

Acknowledgment. The XAFS experiments were performed under the approval of the Photon Factory Proposal Review Committee (2001G308 and 2002G285) and under the approval of the SPring-8 Program Review Committee and the National Institute for Materials Research as Nanotechnology Support Project of the Ministry of Education, Culture, Sports, Science, and Technology (MEXT) (2003A0146-NX-np and 2002B0739-NX-np). The authors are thankful for financial support from the Grant-in-Aid for Scientific Research from MEXT (B1355 5230), Yamada Science Foundation (2000), and Toray Science Foundation (98-3901).

References and Notes

- Izumi, Y.; Oyanagi, H.; Nagamori, H. *Bull. Chem. Soc. Jpn.* **2000**, *73*, 2017–2023.
- Izumi, Y.; Nagamori, H. *Bull. Chem. Soc. Jpn.* **2000**, *73*, 1581–1587.
- Izumi, Y.; Nagamori, H.; Kiyotaki, F.; Minato, T. *J. Synchrotron Radiat.* **2001**, *8*, 605–607.
- Izumi, Y.; Kiyotaki, F.; Nagamori, H.; Minato, T. *J. Electron Spectrosc. Relat. Phenom.* **2001**, *119*, 193–199.
- Izumi, Y.; Kiyotaki, F.; Seida, Y. *J. Phys. Chem. B* **2002**, *106*, 1518–1520.
- Izumi, Y.; Kiyotaki, F.; Minato, T.; Seida, Y. *Anal. Chem.* **2002**, *74*, 3819–3823.
- Izumi, Y.; Kiyotaki, F.; Yoshitake, H.; Aika, K.; Sugihara, T.; Tatsumi, T.; Tanizawa, Y.; Shido, T.; Iwasawa, Y. *Chem. Commun.* **2002**, 2402–2403.
- Izumi, Y.; Kiyotaki, F.; Yoshitake, H.; Aika, K.; Sugihara, T.; Tatsumi, T.; Tanizawa, Y.; Shido, T.; Iwasawa, Y. *Chem. Lett.* **2002**, 1154–1155.
- Izumi, Y.; Kiyotaki, F.; Nagamori, H.; Minato, T. *Stud. Surf. Sci. Catal.* **2003**, *145*, 117–180.
- Izumi, Y.; Masih, D.; Aika, K.; Seida, Y. *J. Phys. Chem. B* **2005**, *109*, 3227–3232.
- Izumi, Y.; Kiyotaki, F.; Minato, T.; Masih, D.; Seida, Y. *Phys. Scr.* **2005**, *T115*, 933–935.

- (12) Glatzel, P.; Jacquamet, L.; Bergmann, U.; de Groot, F. M. F.; Cramer, S. P. *Inorg. Chem.* **2002**, *41*, 3121–3127.
- (13) de Groot, F. *Chem. Rev.* **2001**, *101*, 1779–1808.
- (14) Hamalainen, K.; Siddons, D. P.; Hastings, J. B.; Berman, L. E. *Phys. Rev. Lett.* **1991**, *67*, 2850–2853.
- (15) Heijboer, W. M.; Glatzel, P.; Sawant, K. R.; Lobo, R. F.; Bergmann, U.; Barrea, R. A.; Koningsberger, D. C.; Weckhuysen, B. M.; de Groot, F. M. F. *J. Phys. Chem. B* **2004**, *108*, 10002–10011.
- (16) Stark, W. J.; Wegner, K.; Pratsinis, S. E.; Baiker, A. *J. Catal.* **2001**, *197*, 182–191.
- (17) Gasior, M.; Gasior, I.; Grzybowska, B. *Appl. Catal.* **1984**, *10*, 87–100.
- (18) Gasior, M.; Grzybowska, B.; Haber, J. *React. Kinet. Catal. Lett.* **1980**, *15*, 395–399.
- (19) Bond, G. C.; Konig, P. *J. Catal.* **1982**, *77*, 309–322.
- (20) Wachs, I. E.; Weckhuysen, B. M. *Appl. Catal., A* **1997**, *157*, 67–90.
- (21) Olthof, B.; Khodakov, A.; Bell, A. T.; Iglesia, E. *J. Phys. Chem. B* **2000**, *104*, 1516–1528.
- (22) Gao, X.; Wachs, I. E. *J. Phys. Chem. B* **2000**, *104*, 1261–1268.
- (23) Vittadini, A.; Selloni, A. *J. Phys. Chem. B* **2004**, *108*, 7337–7343.
- (24) Vittadini, A.; Casarin, M.; Selloni, A. *J. Phys. Chem. B* **2005**, *109*, 1652–1655.
- (25) Nielsen, U. G.; Topsoe, N.; Brorson, M.; Skibsted, J.; Jakobsen, H. J. *J. Am. Chem. Soc.* **2004**, *126*, 4926–4933.
- (26) Haber, J.; Kozłowska, A.; Kozłowski, R. *J. Catal.* **1986**, *102*, 52–63.
- (27) Deo, G.; Wachs, I. E. *J. Phys. Chem.* **1991**, *95*, 5889–5895.
- (28) Vejux, A.; Courtine, P. *J. Solid State Chem.* **1978**, *23*, 93–103.
- (29) Kozłowski, R.; Pettifer, R. F.; Thomas, J. M. *J. Chem. Soc., Chem. Commun.* **1983**, 438–439.
- (30) Kozłowski, R.; Pettifer, R. F.; Thomas, J. M. *J. Phys. Chem.* **1983**, *87*, 5172–5176.
- (31) Kozłowski, R.; Pettifer, R. F.; Thomas, J. M. *J. Phys. Chem.* **1983**, *87*, 5176–5181.
- (32) Yoshitake, H.; Sugihara, T.; Tatsumi, T. *Chem. Mater.* **2002**, *14*, 1023–1029.
- (33) Kozłowski, R.; Stadnicka, K. *J. Solid State Chem.* **1981**, *39*, 271–276.
- (34) Bearden, J. A. *Rev. Mod. Phys.* **1967**, *39*, 78–124.
- (35) Nisawa, A.; Okui, M.; Yagi, N.; Nizutani, T.; Yoshikawa, H.; Fukushima, S. *Nuclear Instrum. Methods Phys. Res., Sect. A* **2003**, *497*, 563–568.
- (36) Izumi, Y.; Glaser, T.; Rose, K.; McMaster, J.; Basu, P.; Enemark, J. H.; Hedman, B.; Hodgson, K. O.; Solomon, E. I. *J. Am. Chem. Soc.* **1999**, *121*, 10035–10046.
- (37) Wong, J.; Lytle, F. W.; Messmer, R. P.; Maylotte, D. H. *Phys. Rev.* **1984**, *30*, 5596–5610.
- (38) Evans, H. T., Jr. *Inorg. Chem.* **1966**, *5*, 967–977.
- (39) Yasuda, S.; Kakiyama, H. *X-ray Spectrom.* **1978**, *7*, 23–25.
- (40) Kozłowski, R.; Ziolkowski, J.; Mocala, K.; Haber, J. *J. Solid State Chem.* **1980**, *35*, 1–9.
- (41) Krause, M. O.; Oliver, J. H. *J. Phys. Chem. Ref. Data* **1979**, *8*, 329–338.
- (42) Lytle, F. W.; Greeger, R. B.; Sandstrom, D. R.; Marques, E. C.; Wong, J.; Spiro, C. L.; Huffman, G. P.; Huggins, F. E. *Nuclear Instrum. Methods Phys. Res.* **1984**, *226*, 542–548.
- (43) Eckert, H.; Wachs, I. E. *J. Phys. Chem.* **1989**, *93*, 6796–6805.
- (44) Mikheeva, E. P.; Kachurovskaya, N. A.; Zhidomirov, G. M. *Kinet. Catal.* **2002**, *43*, 223–232.
- (45) Went, G. T.; Leu, L.; Bell, A. T. *J. Catal.* **1992**, *134*, 479–491.
- (46) Jehng, J.; Deo, G.; Weckhuysen, B. M.; Wachs, I. E. *J. Mol. Catal. A* **1996**, *110*, 41–54.
- (47) Khaliullin, R. Z.; Bell, A. T. *J. Phys. Chem. B* **2002**, *106*, 7832–7838.
- (48) Bond, G. C. *Appl. Catal., A* **1997**, *157*, 91–103.
- (49) Went, G. T.; Oyama, S. T.; Bell, A. T. *J. Phys. Chem.* **1990**, *94*, 4240–4246.
- (50) Balikdjian, J. P.; Davidson, A.; Launay, S.; Eckert, H.; Che, M. *J. Phys. Chem. B* **2000**, *104*, 8931–8939.